Int. J. Heat Mass Transfer. Vol. 34, No. 8, pp. 1909–1916, 1991
Printed in Great Britain

0017-9310/91 $3.00+0.00

Pressure drop and mass transfer around perforated turbulence promoters placed in a circular tube

HWA WON RYU,† YOUNG SOON HYEON,‡ DONG IL LEE,‡
HO NAM CHANG†§ and O OK PARK†

† Department of Chemical Engineering, Korea Advanced Institute of Science and Technology, P.O. Box 131, Cheongryang, Seoul 130-650, Korea
‡ Department of Chemical Engineering, Chonnam National University, Kwangju 500-757, Korea

(*Received* 14 *September* 1989 *and in final form* 22 *July* 1990)

Abstract—The friction factors and mass transfer coefficients in a tube with fins of $e/D = 0.1$, 0.2, 0.24 and 0.3 are investigated both experimentally and theoretically in the wide range of Reynolds numbers up to 8000. As expected the friction factor decreased linearly with Reynolds number up to $Re = 200$ and remained nearly constant at $Re > 500$ for all cases of e/D. The distribution of pressure between the fins is measured in detail. The perforated fins are proved to be effective both in reducing loss and in enhancing mass transfer.

1. INTRODUCTION

THE ENHANCEMENT of the heat or mass transfer from the flowing fluid in a channel is important for the design of compact heat exchangers, electrodialysers, and membrane blood oxygenators [1].

Turbulence promoters have been widely used for this purpose. In electrodialysers, for example, the turbulence promoters installed in a channel prevent the formation of the boundary layers and thus they not only improve the mass transfer but also prevent polarization. Most previous investigations were concerned with turbulent flow at high Reynolds number, but it is much more necessary to promote the heat or mass transfer augmentation in the case of laminar flow because this case usually results in low heat or mass transfer. Many types of turbulence promoters have been proposed to see the global mass transfer enhancements, but few studies have been carried out on the distribution of local mass transfer coefficients in the laminar flow with fin-type turbulence promoters. Rowley and Patankar [2] studied the heat transfer in a tube with fins numerically for laminar flow. They showed that although the recirculating flow aids mixing, the heat transfer coefficient often decreases in the laminar flow due to the poor heat exchange between the main stream and the vortices near ribs. Thomas [3] and Miyashita *et al.* [4] used detached turbulence promoters with some clearance between the wall of the channel, and found that the mass transfer increases throughout the channel including the region just after the turbulence promoters, by comparing with the mass transfer in a smooth channel. The perforated fins can be introduced as a compromise between these two types of promoters. In fact, Tanasawa *et al.* [5] used perforated plate promoters to see an increase of heat transfer coefficients at high Reynolds number. In addition, they showed that perforated promoters have an advantage of low pressure drop since the form drag due to the installed promoters can be reduced significantly. Therefore, it may be interesting to perform the mass transfer experiments on flows of low Reynolds number in a tube with perforated and non-perforated fins. In addition, the pressure measurements were carried out to determine the friction loss due to the installation of the fins. Furthermore, theoretical solutions were obtained using a finite difference method in the laminar flow regime and were compared with experimental results.

2. EXPERIMENTAL APPARATUS AND PROCEDURES

2.1. *Pressure measurement*

Figure 1 shows a schematic diagram of the experimental apparatus for pressure measurements. Water

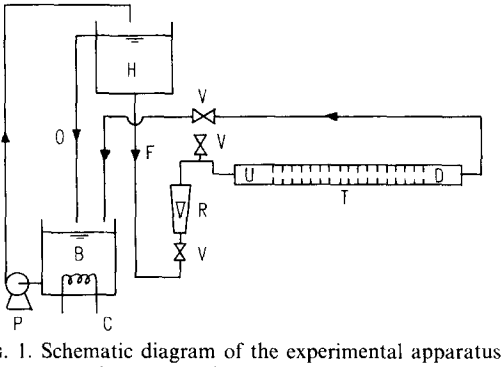

FIG. 1. Schematic diagram of the experimental apparatus: B, bottom tank; D, smooth downstream; F, feed; H, head tank; O, over flow; P, pump; R, rotameter; T, test section for local pressure drop; U, smooth upstream section; V, control valve.

§ Author to whom all correspondence should be addressed.

NOMENCLATURE

A	electrode area [m^2]
C	concentration divided by C_{in} [—]
C_b	bulk concentration [kmol m^{-3}]
C_{in}	inlet concentration [kmol m^{-3}]
C_p	surface pressure coefficient [—]
C_s	concentration at a solid wall [kmol m^{-3}]
D	inside diameter of a tube [m]
D_v	diffusivity [m^2 s^{-1}]
e	height of roughness element [m]
f	friction factor [—]
F	Faraday constant, 96 520 C k mol^{-1}
i	limiting current density [A m^{-2}]
k	local mass transfer coefficient [m s^{-1}]
L	pipe length, $L'D$ [—]
n	valence charge of ion [—]
N	mass flux [kmol m^{-2} s^{-1}]
p	dimensionless pressure, $p'/\rho U^2$ [—]
p_i'	local static pressure [m^2]
p_{i0}'	static pressure at reference tap [N m^{-2}]
Pe	Peclet number, UD/D_v [—]
r	radial coordinate [—]
Re	Reynolds number based on D and U [—]
Sh	Sherwood number, kD/D_v [—]
Sh_m	mean Sherwood number [—]
U	average velocity based on tube diameter [m s^{-1}]
z	axial coordinate [—].

Greek symbols

β	fraction of the perforated area in a fin [—]
ρ	density of fluid [kg m^{-3}]
ϕ	diameter of drilling holes on the ribs [mm] dependent variables $\Psi w/r$, and C [—]
Ψ	stream function, $\Psi'/(DU)$ [—]
ω	vorticity, $\omega' D/U$ [—].

Superscript

$'$	variable with dimensions.

at 25 C was supplied from the constant head tank (H) and passed through the flow control valve (V), rotameter (R) and test section (T). The test section was 2676 mm long and 17 fins were inserted in it equidistantly. The fin-inserted section was preceded by a smooth tube (U) 650 mm long and was followed by a tube (D) of the same length. Total pressure loss was calculated by measuring the pressures just before the first fin and just after the last fin. The local pressure distribution between the ninth and tenth fins was measured using differential manometers that were connected to the 12 tabs as shown in Fig. 2. Carbon tetrachloride or mercury was used as the manometer fluid depending upon the magnitude of the pressure differences. Manometer readings were carefully measured with a cathetometer (Gaertner Scientific Corp., U.S.A.) within the accuracy of 0.01 mm. The inner diameter of the tube was 49.4 mm and the orifice diameters were 19.4, 25.4, 29.4, and 39.4 mm, thus the ratios of the fin height to tube diameter (e/D) were 0.3, 0.24, 0.2, and 0.1, respectively. Both tube and fins were made of acryl and the thickness of the rib was 2.0 mm. The pitch of the fins was fixed at 87 mm. Open area ratios (β), defined by the ratio of the total perforated area to the fin area, of the perforated fins of $e/D = 0.3$ were made 0.08, 0.13, and 0.23, respectively, by drilling holes of 1.6–2.1 mm in diameter on the ribs. Two types of the hole array were made—staggered and in-line type. Detailed configurations of the perforated fins are shown in Fig. 3.

2.2. *Experiment on mass transfer*

The mass transfer experiment was performed by the limiting current method [6] by utilizing the well-

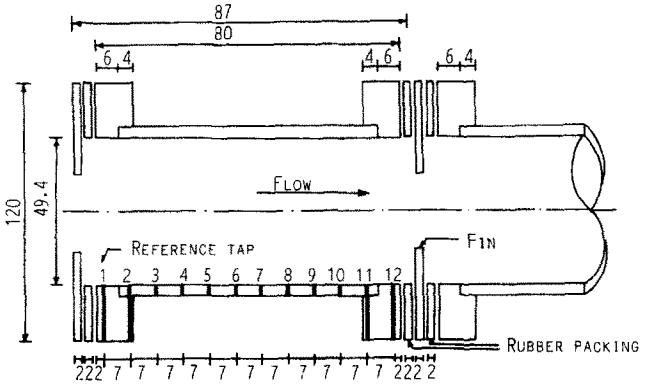

FIG. 2. Details of the test section for local pressure distribution (unit mm).

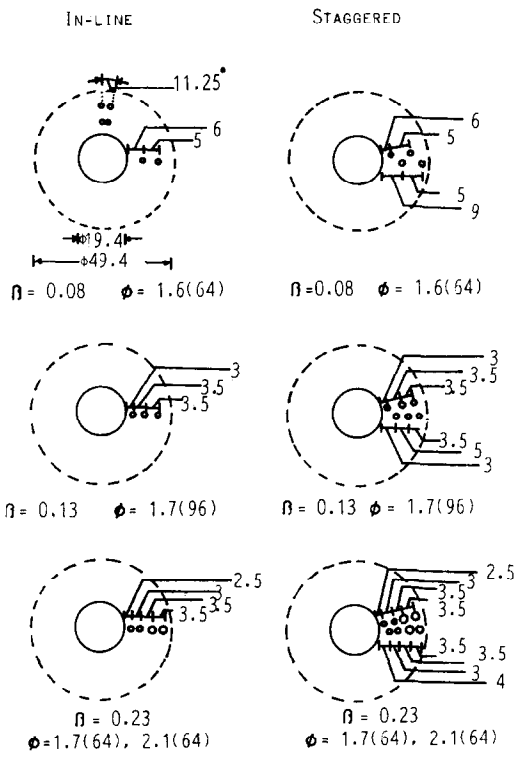

FIG. 3. Configurations of the perforated fins (numbers of the holes are given in parentheses, $e/D = 0.3$, unit mm).

known redox reaction between ferricyanides and ferrocyanides. The electrolytic solution consisted of 0.01 M of $K_3Fe(CN)_6$, 0.01 M of $K_4Fe(CN)_6$ and 1.0 M of NaOH. The concentration of the ferricyanide was checked periodically before each experiment by using the iodometric method [7]. To prevent decomposition of the ferricyanide all experiments were carried out in a dark room with local illumination and nitrogen was continuously bubbled through the fluid at the bottom tank (B in Fig. 1). The experimental apparatus for mass transfer is not presented here but it is similar to the apparatus shown in Fig. 1 with some minor modifications. Equipment for measuring the currents consisted of a d.c. power supply, two multimeters and a control box. Nickel plates 0.1 mm thick were attached to the acryl tube by epoxy resin. Sixteen cathodes 4.72 mm wide were installed and circular teflon sheets 0.45 mm thick were inserted between them for electrical isolation. Great care was paid to ensure smooth conditions at tube walls. Detailed locations of the cathodes are presented in Fig. 4. The test section for mass transfer was located at the same test section for pressure measurement as explained before. The anodes 600 mm in length were installed downstream of the cathodes. The physical properties of the solution used in this experiment and the details of the electric circuit can be found elsewhere [8]. Typical polarization curves were obtained for various Re up to 500 and limiting currents were obtained at above 400 mV. A constant voltage of 600 mV was supplied using a d.c. power supply. At the limiting current the interfacial concentration, C_s, becomes zero, and the mass transfer coefficient is expressed as

$$k = i/(nFC_b - C_s)). \tag{1}$$

The dimensionless mass transfer rate and the Sherwood number can be obtained as

$$Sh = kD/D_v = iD/(nFC_bD_v). \tag{2}$$

3. THEORETICAL CALCULATION

A theoretical study was carried out for the typical module shown in Fig. 5 by a two-dimensional, finite-difference method in a cylindrical coordinate. The flow was assumed to be laminar. It is a somewhat different story to treat a turbulent flow problem with flow separation, which is beyond the scope of this paper. Computations were performed for different values of the Reynolds number and of the geometrical parameter e/D. The flow patterns were assumed to be periodical, while the profiles of concentration were not because mass transfer was assumed to occur at only one section among the repeated ribs. The governing equations for the stream function, vorticity and concentration can be written as follows:

$$\frac{\partial}{\partial r}\left(\frac{1}{r}\frac{\partial \Psi}{\partial r}\right) + \frac{1}{r}\frac{\partial^2 \Psi}{\partial z^2} = -\omega \tag{3}$$

$$v_r\frac{\partial \omega}{\partial r} + v_z\frac{\partial \omega}{\partial z} - \frac{v_r}{r}\omega = \frac{1}{Re}\left(\frac{\partial^2 \omega}{\partial r^2} + \frac{1}{r}\frac{\partial \omega}{\partial r} + \frac{\partial^2 \omega}{\partial z^2} - \frac{1}{r^2}\omega\right) \tag{4}$$

$$v_r\frac{\partial C}{\partial r} + v_z\frac{\partial C}{\partial z} = \frac{1}{Pe}\left(\frac{\partial^2 C}{\partial r^2} + \frac{1}{r}\frac{\partial C}{\partial r} + \frac{\partial^2 C}{\partial z^2}\right). \tag{5}$$

The stream function and the vorticity in the above equations are defined as follows:

$$v_r = -\frac{1}{r}\frac{\partial \Psi}{\partial z}, \quad v_z = \frac{1}{r}\frac{\partial \Psi}{\partial r} \tag{6}$$

$$\omega = \frac{\partial v_r}{\partial z} - \frac{\partial v_z}{\partial r}. \tag{7}$$

The boundary conditions for stream function Ψ are:

(i) at all tube walls

$$\Psi = 0, \quad \frac{\partial \Psi}{\partial n} = 0; \tag{8}$$

(ii) the relations between the inlet and the outlet

$$\Psi_{11}(r) = \Psi_{1W2}(r) \tag{9}$$

$$\Psi_{1N}(r) = \Psi_{1W1}(r); \tag{10}$$

(iii) at the centre of the tube

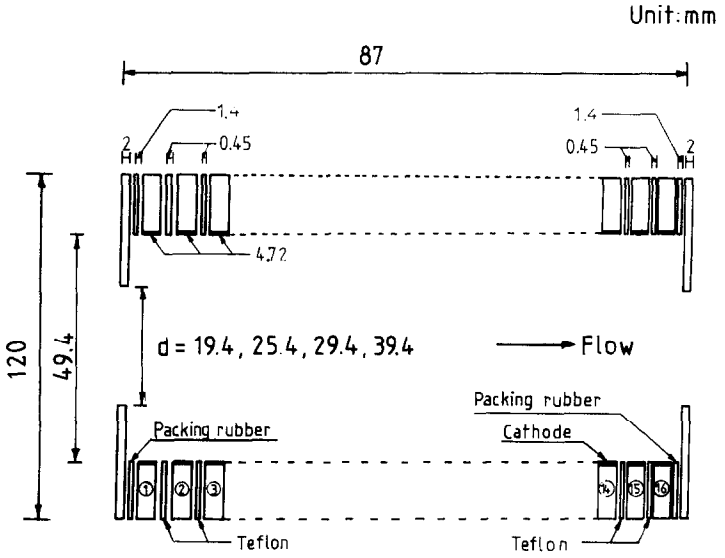

FIG. 4. Details of the test section for local mass transfer (unit mm).

$$\frac{\partial \Psi}{\partial r} = 0. \tag{11}$$

The boundary conditions for concentration C are:

(i) at the inlet

$$C = 1; \tag{12}$$

(ii) at the outlet

$$\frac{\partial C}{\partial z} = 0; \tag{13}$$

(iii) at the conducting tube wall under the condition of limiting current

$$C = 0; \tag{14}$$

(iv) at the non-conducting walls

$$\frac{\partial C}{\partial n} = 0 \tag{15}$$

where n stands for the normal distance from the wall.

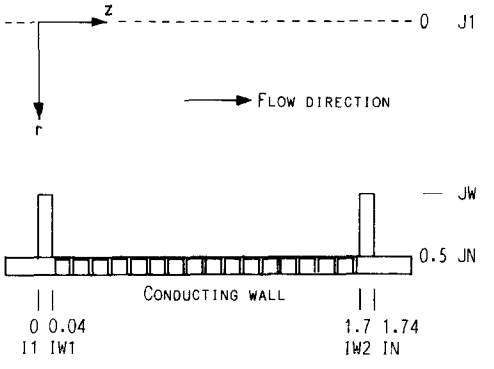

FIG. 5. Model for theoretical analysis of the tube with circular fins (lengths are scaled by inside diameter of the tube).

These three governing equations can be transformed into the following generalized form:

$$a_\phi \left\{\frac{\partial}{\partial z}\left(\phi \frac{\partial \Psi}{\partial r}\right) - \frac{\partial}{\partial r}\left(\phi \frac{\partial \Psi}{\partial z}\right)\right\} - \frac{\partial}{\partial z}\left\{b_\phi r \frac{\partial (c_\phi \phi)}{\partial z}\right\} - \frac{\partial}{\partial r}\left\{b_\phi r \frac{\partial (c_\phi \phi)}{\partial r}\right\} + r d_\phi = 0 \tag{16}$$

where ϕ denotes the dependent variables Ψ, ω/r, and C. The corresponding coefficients a_ϕ, b_ϕ, c_ϕ, and d_ϕ are listed in Table 1. The upwind difference method developed by Gosman *et al.* [9] was also used to solve the above equations. The linear variation of vorticity from the wall to the neighbouring point was assumed. The mesh size ranged from 1/100 near the wall to 1/50 near the centre of the tube in the r-direction and from $h = 1/50$ to 1/10 in the z-direction. The under-relaxation method was used to give a stable solution at the expense of long computation time. From the Navier–Stokes equation the pressure gradient along the z-axis can be obtained as follows:

$$\frac{\partial p}{\partial z} = -\frac{1}{Re}\left(\frac{\partial \omega}{\partial r} - \frac{\omega}{r}\right) - v_r \frac{\partial v_z}{\partial r} - v_z \frac{\partial v_z}{\partial r}. \tag{17}$$

Therefore, the pressure drop along the z-axis can be calculated by integrating the pressure gradient between the neighbouring points as

Table 1. Coefficients of equation (16)

ϕ	a_ϕ	b_ϕ	c_ϕ	d_ϕ
Ψ	0	$1/r^2$	1	$-\omega/r$
ω/r	r^2	r^2	$1/Re$	0
C	1	1	$1/(Re\,Sc)$	0

$$\int_A^B \left(\frac{\partial p}{\partial s}\right) \mathrm{d}s = p_B - p_A \approx \frac{1}{2}\left\{\left(\frac{\partial p}{\partial s}\right)_B\right\}(s_B - s_A) \tag{18}$$

where s is the distance along an integration path. Friction loss was evaluated by the following equation:

$$f = -\Delta p'/(4L'/D)/(\rho U^2/2) = -\Delta p/(2L). \tag{19}$$

The rate of mass transfer at the tube wall is

$$N = -D_v\left(\frac{\partial C}{\partial r}\right) = k(C'_{in} - C'_s). \tag{20}$$

In dimensionless form

$$Sh = kD/D_v = -\left(\frac{\partial C}{\partial r}\right)_{r=0.5}. \tag{21}$$

The mean Sherwood number was defined as

$$Sh_m = \frac{1}{L}\int_0^L Sh\, \mathrm{d}z. \tag{22}$$

4. RESULTS AND DISCUSSION

4.1. *Pressure drop*

Figure 6 shows the relationship between friction factor and Reynolds number in a tube with non-perforated fins with $e/D = 0.10$. The friction factor decreases with the average slope of -1.0 until $Re = 200$ and is almost constant at $Re > 500$. In the cases of $e/D = 0.2$ and 0.3 the friction factors show the same trends with Reynolds number. The slope of the theoretical solutions agrees well with the experiments until about $Re = 200$, but disagrees at larger Reynolds numbers. The reason is that the actual flow pattern becomes unstable at Reynolds numbers above 200, while the theoretical solution is obtained stable due to the assumption of the laminar flow.

The experiments on the effect of perforation were carried out for several kinds of perforated fins with constant e/D ($=0.3$) and the results plotted in Fig. 7. One can easily find that the decreasing pattern of friction factor is similar to the non-perforated ones, however, the perforated fins have lower friction factors. The friction factor at $\beta = 0.23$ does not seem to reach a constant value even for the large Reynolds number region. Though the friction factors are still larger than those of smooth tubes they significantly decrease as β increases in the high Reynolds number range. One can see that tubes with staggered perforated fins have slightly higher friction factors than those with in-line perforated fins at Reynolds numbers higher than 50.

For the qualitative explanation on the differences in friction factors it is necessary to investigate the local pressure distributions between ribs, which can be either non-perforated or perforated, in detail. The local pressure distribution in a section between the two fins can be represented by the surface pressure coefficient (C_p) at the ith tap which is defined as follows:

$$C_p = (p'_i - p'_0)/(\rho U^2/2) \tag{23}$$

where p'_0 is the static pressure at the reference tap (first tap as shown in Fig. 2), p'_i the ith local static pressure, and U the average velocity based on the diameter of a tube. The dependence of C_p on e/D at $Re = 200$, $\beta = 0$ is found in Fig. 8. When $e/D = 0.1$, 0.2, and 0.24, C_p shows a little scattered pattern, but it is quite gradual. A big difference can be found in the local pressure distribution for $e/D = 0.3$ where C_p tends to have a minimum point near the centre because of the recirculating flows generated between the ribs, as demonstrated in Fig. 9. As Chang [10] pointed out

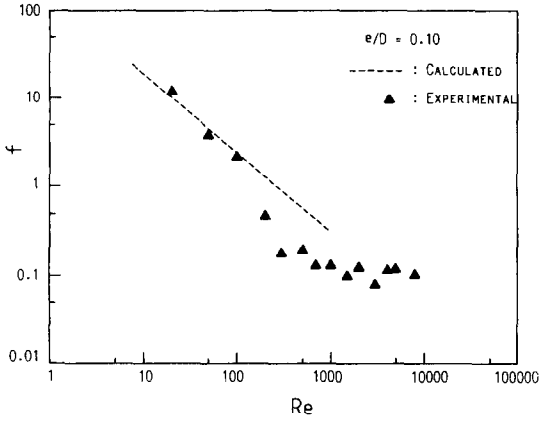

FIG. 6. Friction factor for a tube with non-perforated fins ($e/D = 0.1$).

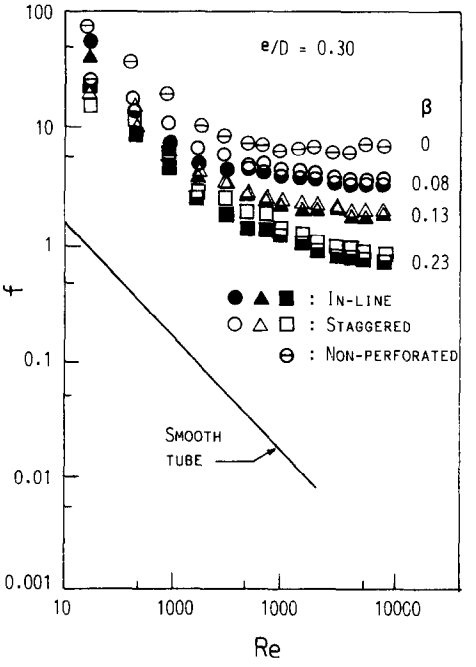

FIG. 7. Friction factor for a tube with perforated fins.

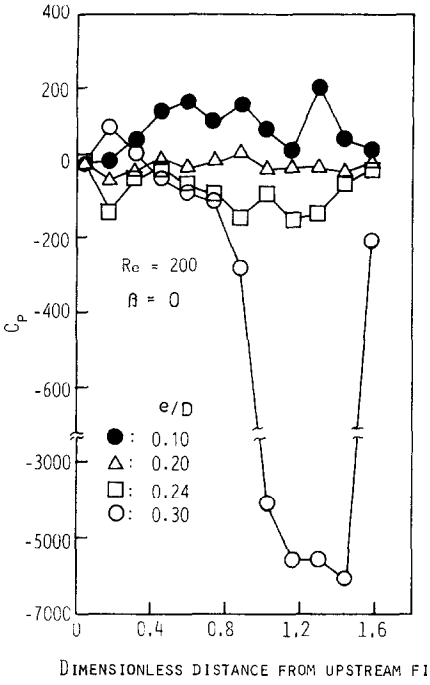

FIG. 8. Distribution of the surface pressure coefficient at $Re = 200$ for the case of non-perforated fins as functions of dimensionless distance from upstream fin scaled by inside diameter of the tube.

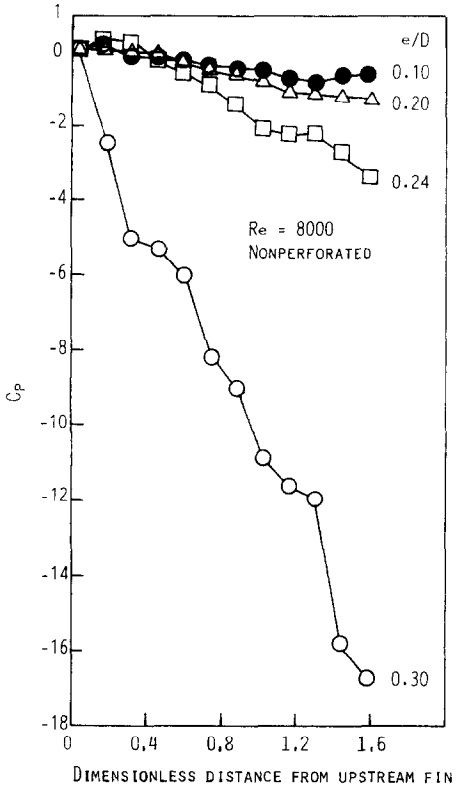

FIG. 10. Distribution of the surface pressure coefficient at $Re = 8000$ for the case of non-perforated fins as functions of dimensionless distance from upstream fin scaled by inside diameter of the tube.

before, the low pressure near the centre of the bottom and the high pressure at the corner are typical of a single, stable vortex generated. The pressure recovers gradually at the last tap near the neighbouring fin even though the pressure recovery is not good at high e/D as shown in Fig. 8. On the other hand at a high Reynolds number of 8000, the pressure between non-perforated fins decreases very slowly and linearly for all e/D as is presented in Fig. 10, and one can easily find that the pressure is not recovered at all at the last tap. This kind of stable pressure distribution results in the almost constant friction factor at high Reynolds number. Figure 11 shows the effect of the open area ratio, β, on pressure distribution at a low Reynolds number of 200. The distribution of the local pressure in tubes with perforated fins shows a great difference from those with non-perforated fins indicating that a recirculating vortex disappears by the perforated holes. From a dye-injection experiment it was confirmed that some portion of the fluid passed through the holes perforated on the ribs, and thus the vortex disappeared resulting in an unstable flow pattern. Figure 12 also shows the distribution of the local pressure in a tube with perforated fins at a high Reynolds number of $Re = 8000$ and $e/D = 0.3$. The local pressure distribution for several β shows a similar tendency to the non-perforated case except the amount of the permanent pressure losses.

4.2. *Mass transfer*

Figure 13 shows a comparison of the distribution of the local mass transfer coefficients at various β and at nearly the same Reynolds numbers. Comparing with the data of the non-perforated fins, one can find

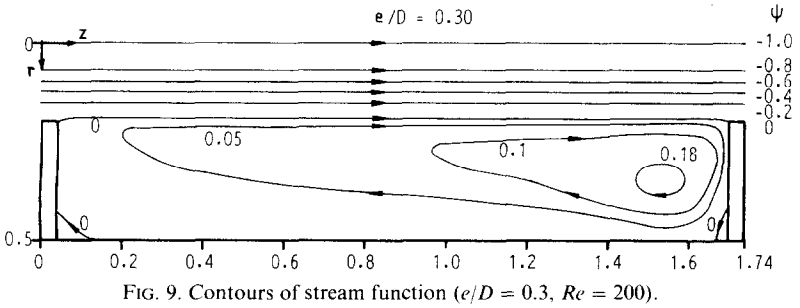

FIG. 9. Contours of stream function ($e/D = 0.3$, $Re = 200$).

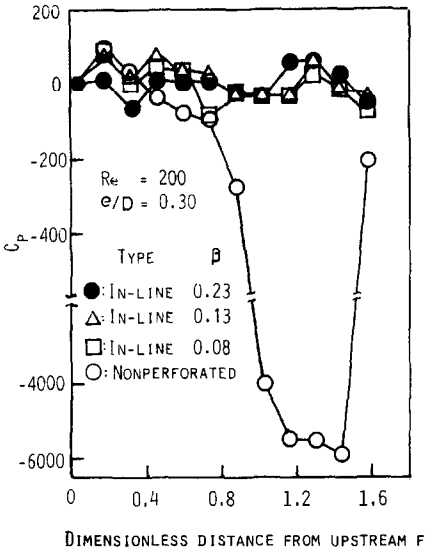

FIG. 11. Distribution of the surface pressure coefficient at $Re = 200$ and $e/D = 0.3$ for the case of perforated fins as functions of dimensionless distance from upstream fin scaled by inside diameter of the tube.

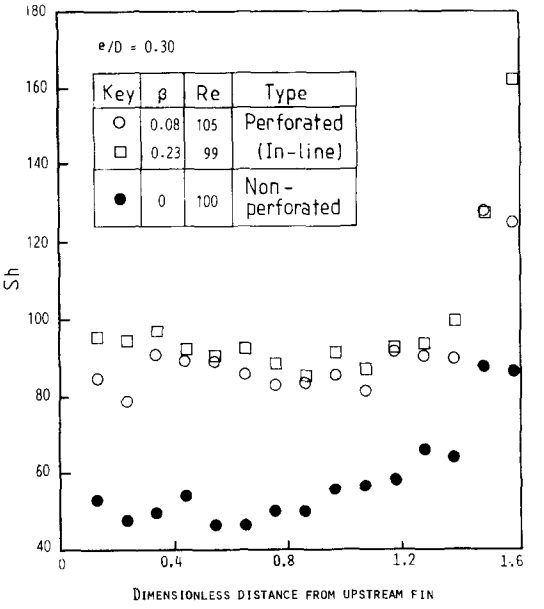

FIG. 13. Dependence of the local Sherwood number on open area ratio as functions of dimensionless distance from upstream fin scaled by inside diameter of the tube.

that mass transfer is increased significantly by perforation. The reason for this is that the fluids that pass through the the perforated holes break both the recirculating flow and the concentration boundary layer near the tube wall. The mean Sherwood numbers obtained by both experiment and theory are shown in Fig. 14 for non-perforated cases ($e/D = 0.1$). Sherwood number increases with Re^a with $a = 0.37$ until a moderate Reynolds number and thereafter approaches a constant value. This tendency is also found for larger e/D at a slightly larger value of a ($a = 0.43$ when $e/D = 0.3$). Figure 15 shows the enhancement of the mean Sherwood numbers by perforation at $e/D = 0.3$. For comparison the mean Sherwood number for the inlet section of the same length as the fin pitch used in this experiment is also presented as a dotted line in the figure [11]. One can see that the perforated fins are superior to both the non-perforated fins and the entrance section of a smooth tube in mass transfer. The non-perforated fins, however, are still effective for promotion of mass transfer com-

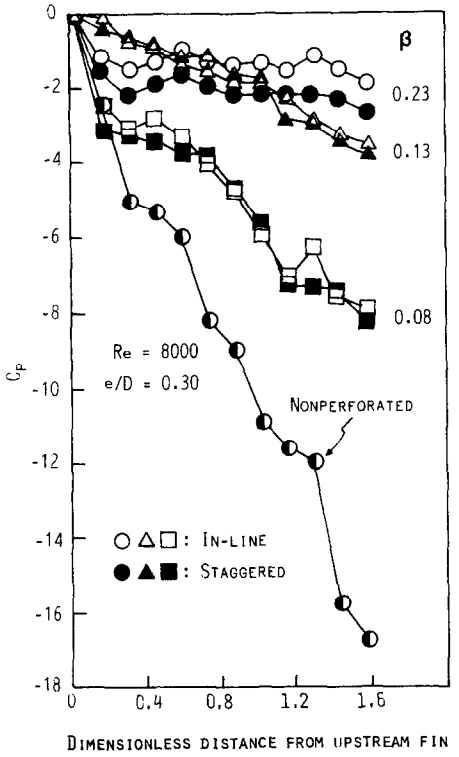

FIG. 12. Distribution of the surface pressure coefficient at $Re = 8000$ and $e/D = 0.3$ for the case of perforated fins as functions of dimensionless distance from upstream fin scaled by inside diameter of the tube.

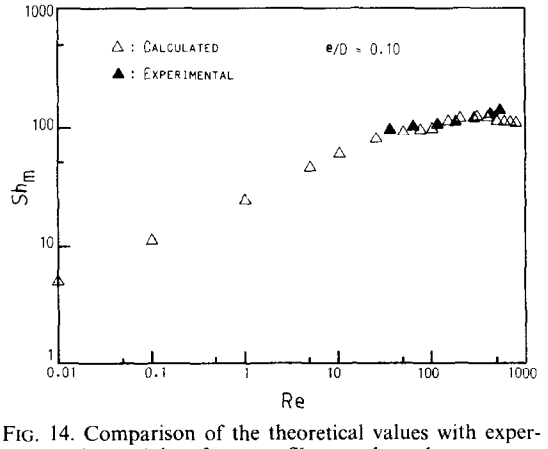

FIG. 14. Comparison of the theoretical values with experimental data for mean Sherwood number.

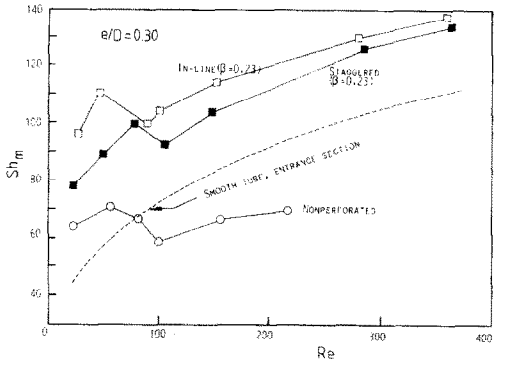

FIG. 15. Dependence of the mean Sherwood number on fin type.

pared with the lower limit of the Graetz problem of which the limiting value of Sh is 3.24 [11].

5. CONCLUSIONS

Friction factors and mass transfer coefficients in a tube with fins of $e/D = 0.1$, 0.2, 0.24, and 0.3 were investigated in the Reynolds number range up to 8000. Comparing the results of the theory and experiment we found that the flow becomes unstable above $Re = 200$. The local distribution of the pressure between the neighbouring fins was investigated in detail and it was found that the flow through the holes in the perforated fins breaks the recirculating vortices between the fins and thus the friction loss is reduced, and also it reduces the concentration boundary layer near the tube wall so that the mass transfer is enhanced. The detailed configuration of perforation does not have much effect on both friction factor and the mass transfer, however, the in-line type is thought to be a little better than the staggered one.

Acknowledgements—Two of the authors (H. W. Ryu and D. I. Lee) gratefully acknowledge the financial support of this work by the Korea Science and Engineering Foundation.

REFERENCES

1. Ho Nam Chang and Joong Kon Park, *Handbook of Heat and Mass Transfer Operations* (Edited by N. P. Cheremisnoff), Vol. II. Gulf, Houston, Texas (1986).
2. G. J. Rowley and S. V. Patankar, Analysis of laminar flow heat transfer in tubes with internal circumferential fins, *Int. J. Heat Mass Transfer* **27**, 553–560 (1984).
3. D. G. Thomas, Forced convection mass transfer, Part III. Increased mass transfer from a flat plate caused by the wake from cylinders located near the edge of the boundary layer, *A.I.Ch.E. Jl* **12**, 124–130 (1966).
4. H. Miyashita, Y. Shiomi and K. Wakabayashi, *Kagaku Kogaku Ronbunshu* **7**, 349–354 (1981).
5. I. Tanasawa, S. Nishio, K. Takano and M. Toda, Enhancement of forced-convection heat transfer in a rectangular channel using turbulence promoters, *J. Soc. Mech. Engng Japan* (in Japanese) **49B**, 676 (1983).
6. H. N. Chang, H. W. Ryu, D. H. Park, Y. S. Park and J. K. Park, Effect of external laminar channel flow on mass transfer in a cavity, *Int. J. Heat Mass Transfer* **30**, 2137–2149 (1987).
7. I. M. Kolthoff and R. Belcher, *Volumetric Analysis*, Vol. III. Interscience, New York (1957).
8. D. H. Kim, I. H. Kim and H. N. Chang, Experimental study of mass transfer around a turbulence promoter by the limiting current method, *Int. J. Heat Mass Transfer* **26**, 1007–1016 (1983).
9. A. D. Gosman, W. M. Pun, A. K. Runchal, D. B. Spalding and M. Wolfshein, *Heat and Mass Transfer in Recirculating Flows*. Academic Press, New York (1969).
10. P. K. Chang, *Separation of Flow*. KIST Press, Seoul (1978).
11. V. G. Levich, *Physicochemical Hydrodynamics*. Prentice-Hall, Englewood Cliffs, New Jersey (1962).

PERTE DE PRESSION ET TRANSFERT DE MASSE AUTOUR DE PROMOTEURS PERFORES DE TURBULENCE PLACES DANS UN TUBE CIRCULAIRE

Résumé—Les coefficients de frottement et de transfert de masse dans un tube ayant des ailettes de $e/D = 0{,}1$; 0,2; 0,24 et 0,3 sont étudiés expérimentalement et théoriquement dans un large domaine de nombre de Reynolds jusqu'à 8000. Comme prévu le coefficient de frottement décroit linéairement quand le nombre de Reynolds augmente jusqu'à $Re = 200$ et reste à peu près constant pour $Re > 500$ dans tous les cas de e/D. La distribution de pression entre les ailettes est mesurée en détail. Les ailettes perforées sont efficaces à la fois pour la réduction de la perte de pression et pour l'accroissement de transfert de masse.

DRUCKABFALL UND STOFFÜBERGANG IN DER NÄHE VON PERFORIERTEN TURBULENZERZEUGERN IN EINEM KREISROHR

Zusammenfassung—Die Reibungsbeiwerte und die Stoffübergangskoeffizienten in einem Rohr mit Rippen ($e/D = 0{,}1$; 0,2; 0,24; 0,3) werden in einem weiten Bereich der Reynolds-Zahl (bis zu 8000) experimentell und theoretisch untersucht. Wie erwartet, nehmen für alle Werte von e/D die Reibungsbeiwerte bis zu $Re = 200$ linear mit der Reynolds-Zahl ab und bleiben für $Re > 500$ annähernd konstant. Die Druckverteilung zwischen den Rippen wird ausführlich gemessen. Die perforierten Rippen erweisen sich sowohl bei der Verminderung des Druckverlustes als auch bei der Intensivierung des Stoffübergangs als wirkungsvoll.

ПЕРЕПАД ДАВЛЕНИЯ И МАССОПЕРЕНОС ВОКРУГ ПЕРФОРИРОВАННЫХ ТУРБУЛИЗАТОРОВ, НАХОДЯЩИХСЯ В ТРУБЕ КРУГЛОГО СЕЧЕНИЯ

Аннотация—Экспериментально и теоретически исследовались коэффициенты трения и массопереноса в трубе с ребрами, у которых $e/D = 0{,}1$; 0,2; 0,24 и 0,3, в широком диапазоне изменения числа Рейнольдса вплоть до значений 8000. Как и ожидалось, коэффициент трения линейно уменьшался для значений числа Рейнольдса вплоть до $Re = 200$ и оставались почти постоянными при $Re > 500$ для всех значений e/D. Детально промерено распределение давлений между ребрами. Показано, что перфорированные ребра могут эффективно использоваться для уменьшения потерь давления и интенсификации теплопереноса.